Supporting Information

Tuning 2D Perovskite-Graphene Layered Composite for Photocatalysis

Haozhe Zhang[a], Yanjie Wang[a], [b], Wentian Niu[a], Tatchamapan Yoskamtorn[a], Mingyu Luo [a], Robert Tayler[c], Sarah Day[d], Shik Chi Edman Tsang[a]*

[a]Wolfson Catalysis Centre, Department of Chemistry, University of Oxford, Oxford, OX1 3QR, UK;
[b]CAS Key Laboratory of Nanosystem and Hierarchical Fabrication, National Centre for Nanoscience and Technology, Beijing 100190, China
[c]Clarendon Laboratory, Department of Physics, University of Oxford; Oxford, OX1 3PU, UK
[d]Diamond Light Source Ltd., Harwell Science and Innovation Campus; Didcot OX11 0DE, UK

* E-mail: edman.tsang@chem.ox.ac.uk

Experimental Section

Materials and reagents

Rubidium carbonate (Rb_2CO_3, >99%), praseodymium oxide (Pr_6O_{11}, >99.996%), neodymium nitrate hexahydrate (Nd_2O_3, >99.9%), lanthanum oxide (La_2O_3, >99.96%), niobium oxide (Nb_2O_5, >99.9%), graphene oxide (1 mg/mL), Tetrabutylammonium hydroxide (TBAOH, ~40% in H_2O) and Poly (diallyldimethylammonium chloride) solution (MW <100000, 35 wt. %) and methanol were purchased from Sigma-Aldrich Co. LLC. All of above chemical reagents were utilised directly without any further purification. Deionised water was used in this experiment.

Layered perovskite $RbLnNb_2O_7$ (Ln = La, Pr and Nd) synthesis

All the materials were synthesised by a ceramic solid-phase synthesis method, which is referenced to the literature studies of the related materials.[1,2] Firstly, La_2O_3/Pr_6O_{11}/Nd_2O_3 and Nb_2O_5 was dried at 900 °C before being used. After that, suitable quantity of metal oxides was ground together with Rb_2CO_3. A 50% excess amount of Rb_2CO_3 was added to compensate for the loss during calcination because of its volatility at high temperature. The mixtures were then heated at 1123 K for 12 h and re-ground. Samples of resulting powder was heated with air flow for 48 h at 1273 K and further 48 h at 1323 K in a muffle furnace. Finally, all the collected layered perovskite samples were washed by ultrasonicating with deionised water for several times to remove any remaining Rb oxides and then dried for 24 h at 333K in a vacuum oven.

Perovskite nanosheets synthesis

Perovskite nanosheets were synthesised by protonating and exfoliating layered perovskite $RbLnNb_2O_7$ (Ln = La, Pr and Nd) with acid and bulky organic molecules, respectively.[3,4] Firstly, the crystallined layered perovskites $RbLnNb_2O_7$ were stirred with 6 M of HNO_3 solution at 333 K for 7 days. Rb^+ in the interlayer space was replaced by protons. The collected powder samples were washed with deionised water until the pH = ~7. Then the resulting product $HLnNb_2O_7$ (Ln = La, Pr and Nd) was dried for 48 h in a vacuum desiccator at room temperature. Then, the as-prepared protonated perovskites $HLnNb_2O_7$ were exfoliated with Tetrabutylammonium hydroxide (TBAOH). Typically, 0.1 g of $HLnNb_2O_7$ powder were added in 0.025 M of 100 ml TBAOH solution and stirred for 14 days. Additionally, the exfoliation process was under assistance of sonication every day. The separation from unexfoliated powder was performed by spontaneous precipitation for 1 day and the supernatant was used as the nanosheet suspension (concentration ~0.5 g/L). The perovskite nanosheets were washed with water several times and dried at room temperature.

Preparation of rGO/PDDA

60 mg of graphene oxide in 20 mL of deionised water was stirred with 800 μl of PDDA for 1 h. Then the solution was heated to 363 K under reflux for 12 hours. Solution was centrifuged at 12,000 rpm for 45 minutes, and the upper layer solution was removed. This step was repeated for several times to remove extra PDDA. Finally, the product was dried at 333 K for 24 h in a vacuum oven.

Synthesis of rGO/LNO, rGO/PNO and rGO/NNO nanohybrids

The typical procedure for nanohybrids was conducted as follows: 1 mg of rGO/PDDA was added in deionised water, then followed by the addition of 20 mL of perovskite nanosheet suspension under stirring. This procedure yielded flocculated sediment as a result of the electrostatic interaction of the perovskite nanosheet and rGO/PDDA. The resulting mixture was placed under UV light with continuous stirring to remove PDDA. Finally, the solid was washed with deionised water and collected by centrifugation at 12,000 rpm for 1 h.

Characterisation of materials

The synthesised materials were characterised by X-ray powder diffraction (XRD) data collected at I11 Diamond light source. All structures were refined by Rietveld analysis using j-Edit and TOPAS program. UV-vis absorption spectra were obtained by a reflection method using a PerkinElmer Lambda UV-visible spectrometer. Transmission electron microscopy (TEM) and high-angle annular dark-field scanning transmission electron microscopy (HAADF-STEM) images were obtained using JEOL JEM-2100 and JEOL ARM-200F analytical electron microscopes operating at 200 kV. Infrared spectra were collected with a Nicolet iS50 FT-IR spectrophotometer from thermo scientific. XPS analysis was carried out on the Casa XPS. The fluorescence lifetimes were measured by a bespoke micro-photoluminescence setup, in which a Ti-Sapphire laser with wavelength of 266 nm, pulse duration of 150 fs and repetition rate of 76 MHz, and spectrometer was used as a monochromator before passing the selected signal to a photomultiplier tube (PMT) detector for the time-resolved analysis.

Photocatalytic hydrogen production

Photocatalytic experiments were performed under a 300 W xenon lamp (Sciencetech, Canada) as a light source and started from the room temperature. 20 mg of photocatalysts ($LnNb_2O_7$ or rGO/$LnNb_2O_7$) was dispersed in 10 mL of aqueous solution with 10 vol% methanol as a hole scavenger, and it was placed in an autoclave. The autoclave was evacuated and purged 10 times with Ar gas. The mixture then was

irradiated under 250 rpm stirring speed for 1 h under 2 bar of 91 cm^3 Ar gas. The distance between light source and autoclave window was kept at 15 cm. Gas samples were analysed with a gas chromatograph (Agilent Technologies 7890B GC system) equipped with a thermal conductivity detector (TCD). The recycle experiments of the photocatalysts were measured over 4 h with four cycles. Each recycle was done by evacuating and purging with Ar gas, in order to remove the residual hydrogen gas in the autoclave. And then the photocatalytic measurement was repeated.

Density functional theory calculation

The first principles calculations based on DFT were performed using the Vienna ab initio simulation package (VASP, version 5.44).[5] The Perdew-Burke-Ernzerhof (PBE) exchange-correlation functional within the generalized gradient approximation (GGA) was used to describe the exchange-correlation energy.[6] The plane wave cutoff energy was 450 eV. Geometries were converged to 10^{-7} eV in electric relaxation energy and 0.01 eV/Å in ion relaxation energy. A vacuum layer of 15 Å was used to avoid the periodic interactions.

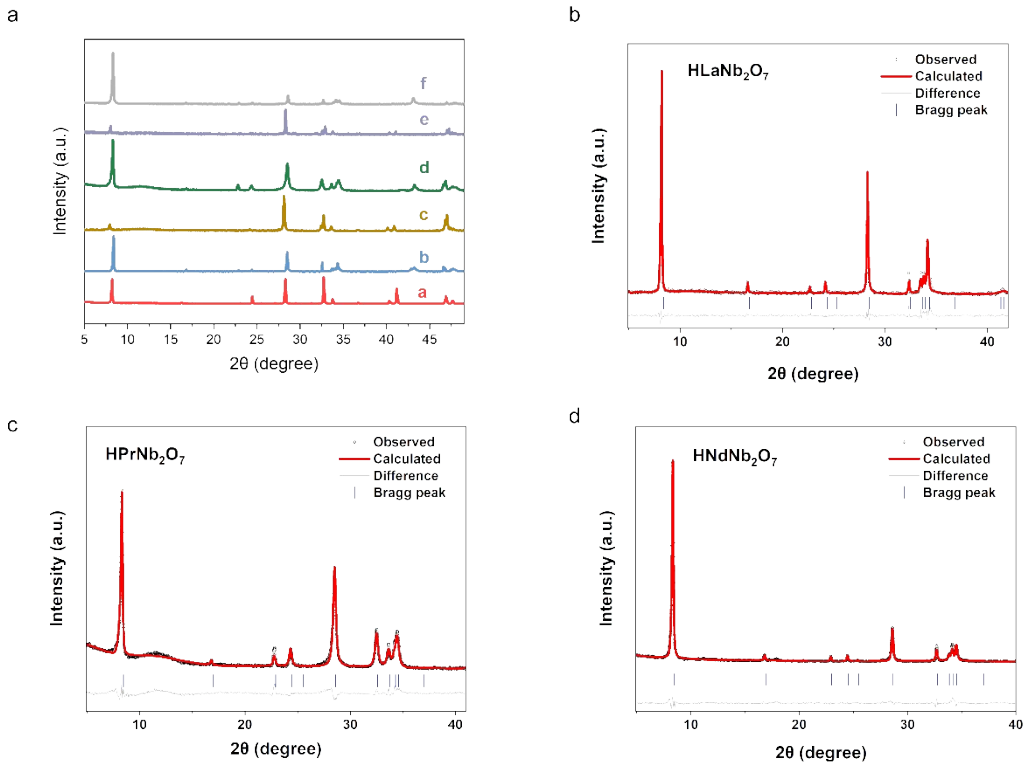

Figure.S1: a) powder XRD pattern of a: $RbLaNb_2O_7$, b: $HLaNb_2O_7$, c: $RbPrNb_2O_7$, d: $HPrNb_2O_7$, e: $RbNdNb_2O_7$, f: $HNdNb_2O_7$; b) Simple Rietveld refinement patterns of $HLaNb_2O_7$ with final reliability factor R*wp* = 14.69%, lattice parameters of a = 3.8918 *Å*, c = 10.5558 *Å*; c) Simple Rietveld refinement patterns of $HPrNb_2O_7$ with final reliability factor R*wp* = 8.59%, lattice parameters of a = 3.8783 *Å*, c = 10.4490 *Å*; d) Simple Rietveld refinement patterns of $HNdNb_2O_7$ final reliability factor R*wp* = 4.69%, lattice parameters of a = 3.8654 *Å*, c = 10.4848 *Å*

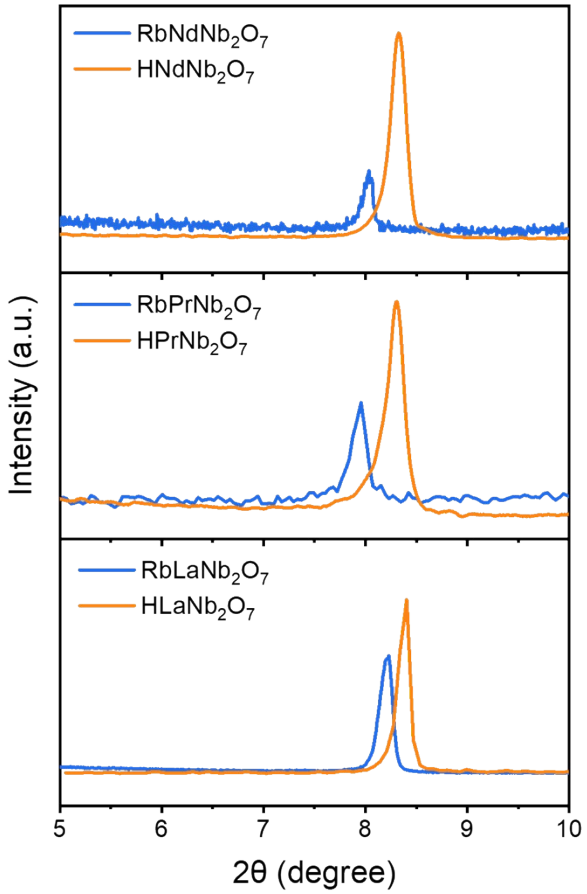

Figure.S2: Diffraction peak (001) in XRD patterns of $RbLnNb_2O_7$ and $HLnNb_2O_7$. The blue peaks at 2θ = ~8.0° represent peak (001) of $RbLnNb_2O_7$ (Ln = La, Pr, Nd), and orange peaks at 2θ = ~8.4° represent peak (001) of $HLnNb_2O_7$. Thus, the (001) peak position can indicate the interlayer space of layered perovskite.[7]

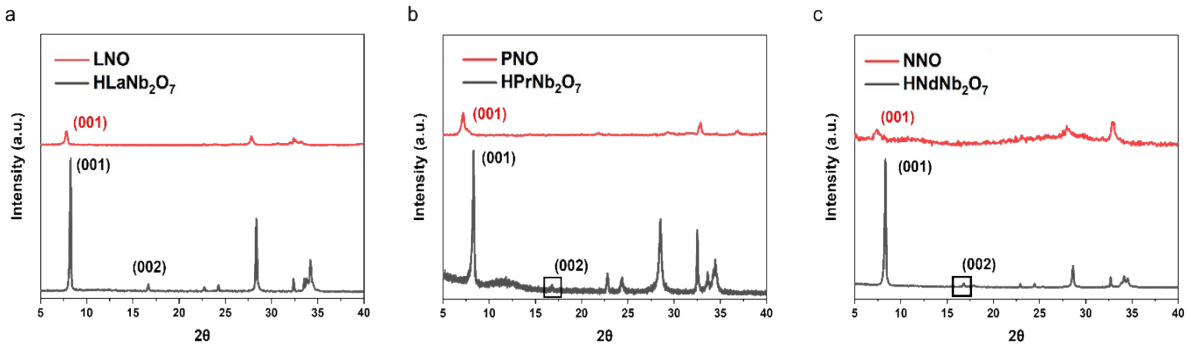

Figure.S3: XRD pattern of a) $HLaNb_2O_7$ and LNO; b) $HPrNb_2O_7$ and PNO; c) $HNdNb_2O_7$ and NNO.

The XRD patterns of $HLnNb_2O_7$ (black line) show a good material crystallinity, which also demonstrate a significantly reduced intensity of (001) peak with obvious shifts to lower angles. This is because the successful exfoliation reduced the crystallinity of layered perovskites, and TBA^+ intercalation can increase interlayer space and create disorder due to its bulky molecular size.[3,8,10]

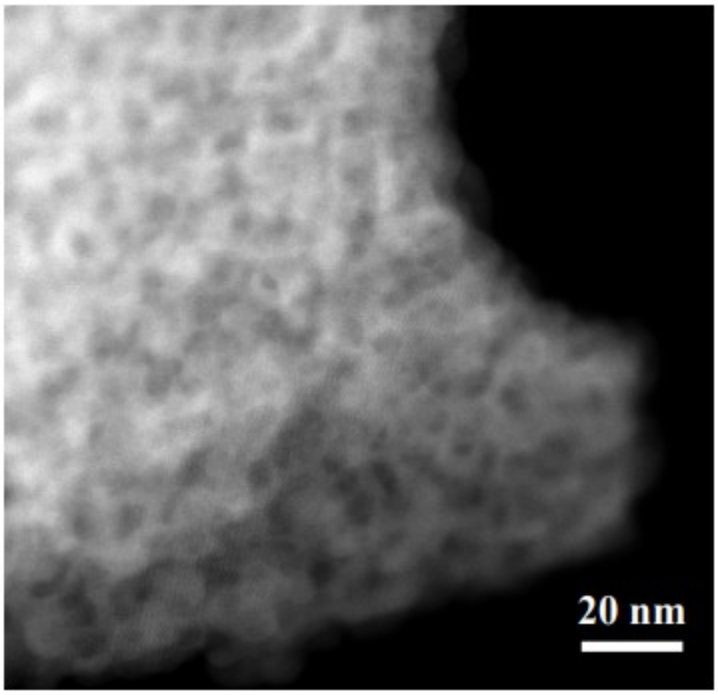

Figure.S4: TEM images of $RbNdNb_2O_7$. The blurred and brightly white part of the image is due to the difference in thickness of the layered perovskite.

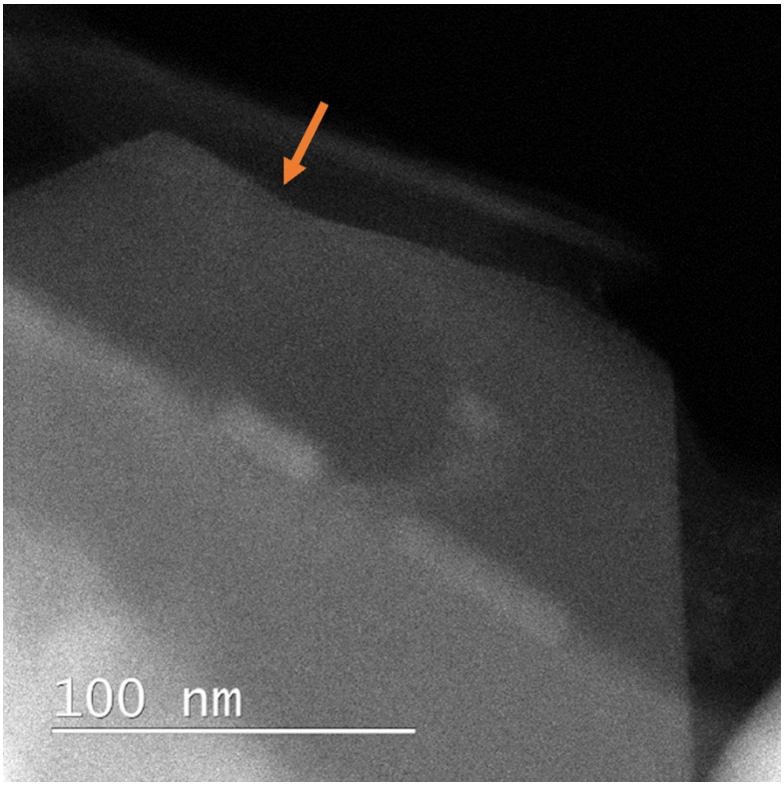

Figure.S5: TEM shows a transparent and plan image of NNO nanosheet. The orange arrow points out the wrinkled portion of the flexible nanosheet edge. [8,9] It demonstrates that NNO perovskite nanosheets are successfully fabricated through TBAOH exfoliation method.

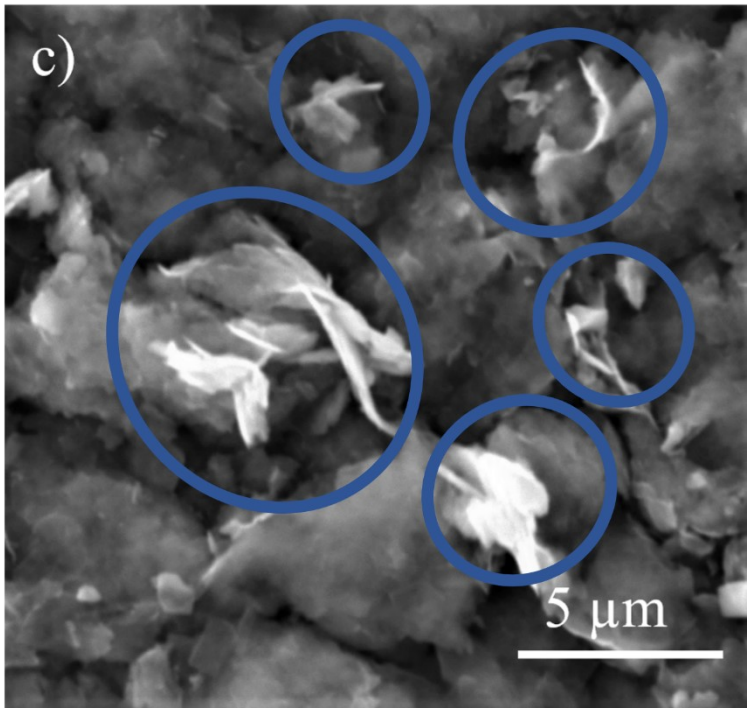

Figure.S6: SEM image of NNO of the sheet-like structure, which is pointed out by blue circles.

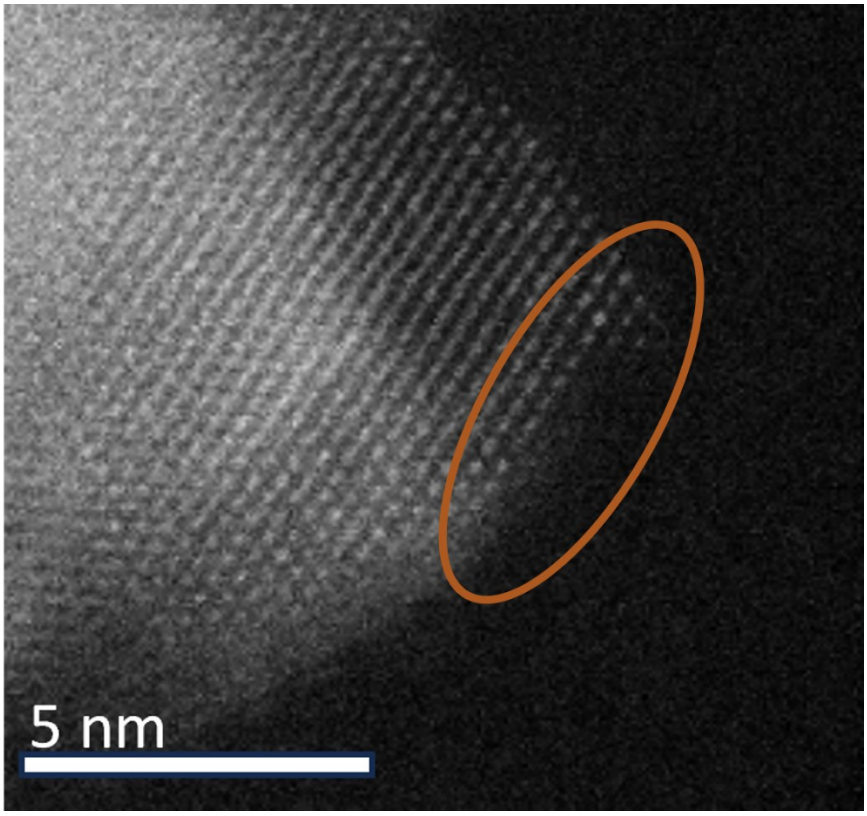

Figure.S7: HADDF-STEM image of enlarged NNO monolayer showing a very crystalline structure. The damage edge of nanosheets is caused by the exfoliation process, which is pointed out by an orange circl

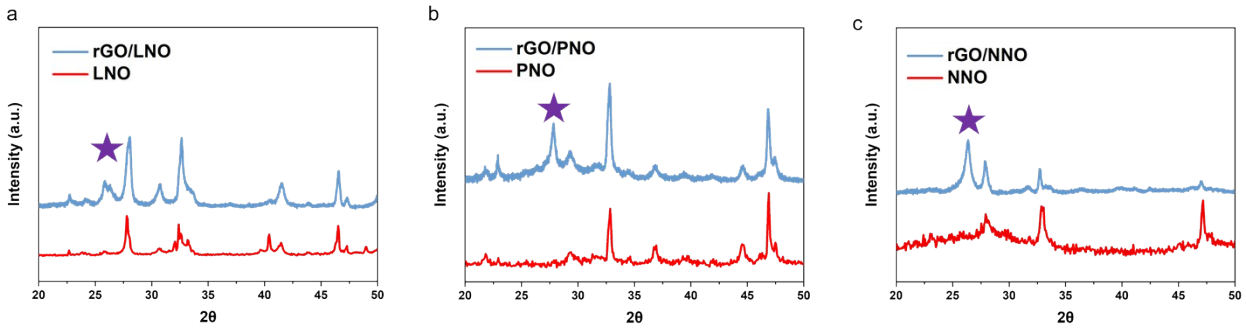

Figure.S8: XRD patterns of a) LNO and rGO/LNO; b) PNO and rGO/PNO; c) NNO and rGO/NNO.

The * label represents the graphitic peak position. It confirms that rGO/perovskite nanosheet composites without any detectable impurities and perovskite nanosheets are stable against decomposition after anchoring on rGO.

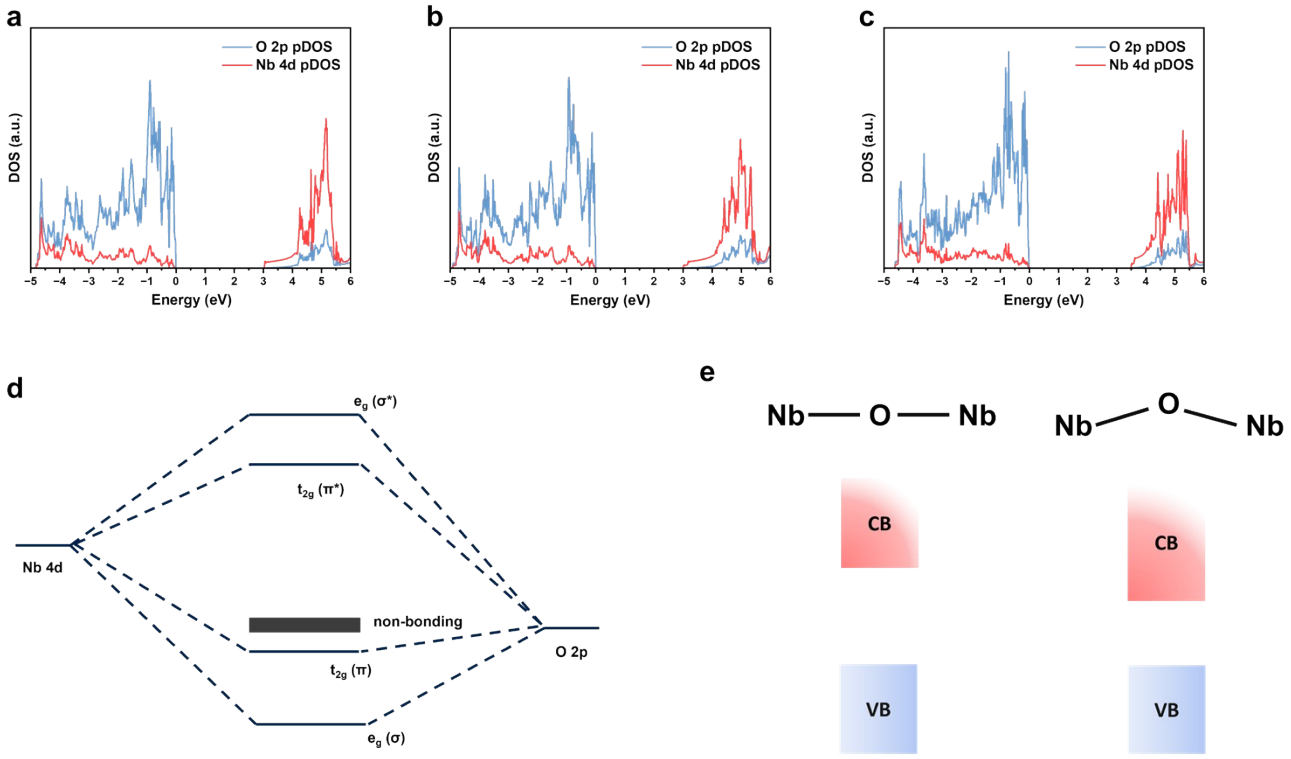

Figure.S9: Calculated pDOS of a) LNO b) PNO and c) NNO perovskite nanosheet by non-SOC DFT-D3+U method (4.0 eV Hubbard U Correction on Nb), and the calculated PNO bandgap (2.96 eV) is lower than that of LNO (3.02 eV), which aligns with our experimental results; d) Molecular orbital of NbO_6 in perovskite, which shows that O 2p non-bonding orbitals are VB maximum and Nb π antibonding represents CB minimum; e) When Nb-O-Nb bond angle reduces, the bandgap shrinks because t_2g (π*) is stabilized.[11,12,13]

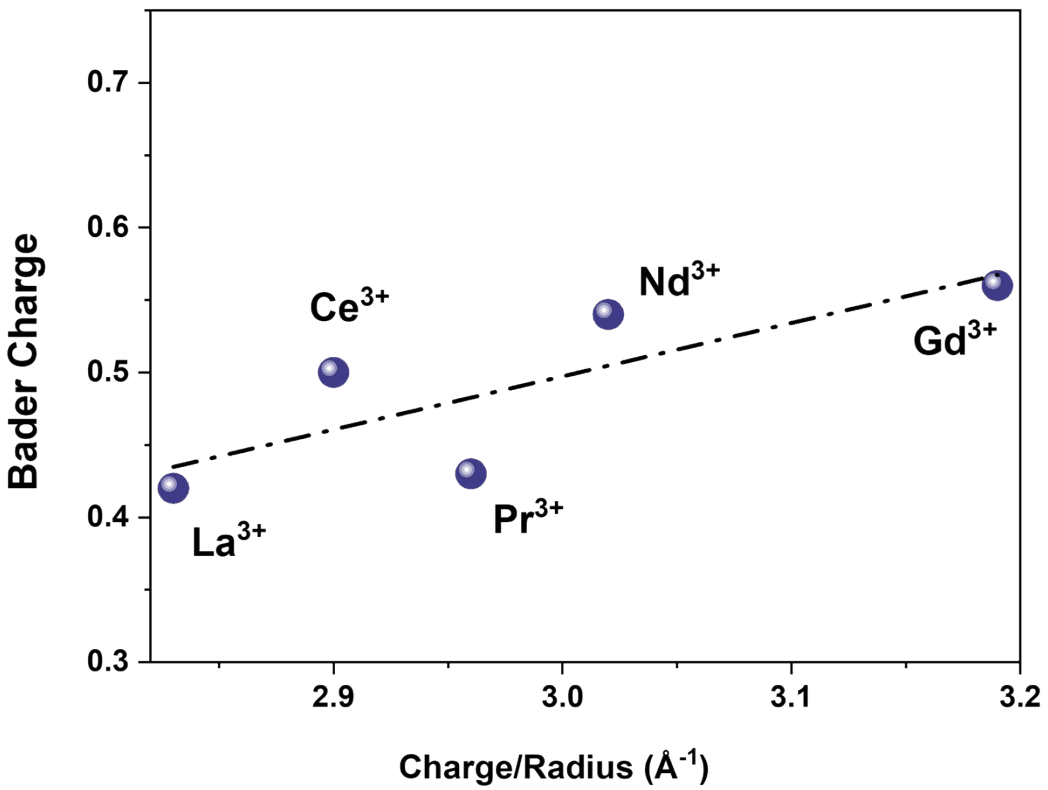

Figure S10: Calculated Bader Charge on oxygen atoms for rGO/LnNO in function of charge density of A.

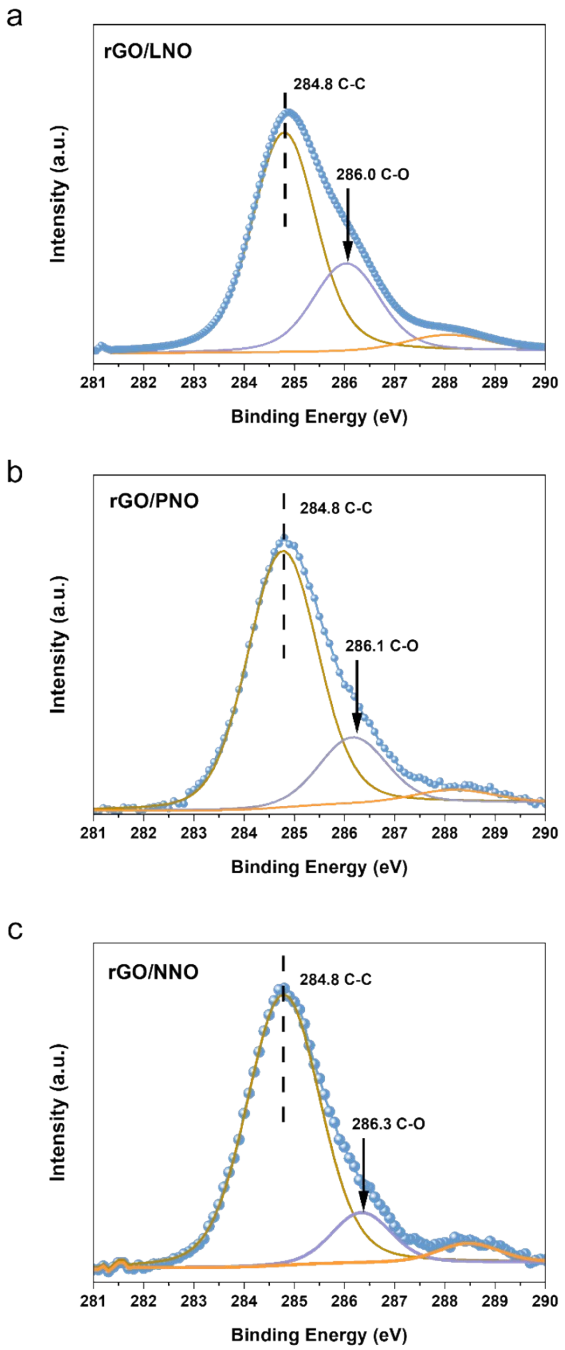

Figure.S11: C 1s XPS of rGO/LNO, rGO/PNO and rGO/NNO showing no change in advantitious C in C-C (284.8 eV). However, ~ 286 eV of graphitic C1s region indicates the progressive shift to higher binding energy from rGO/ LNO to rGO/PNO and rGO/NNO due to increasing h^+ (holes) residence.[14,15,16] as excited electrons are transferred through the C_g-O interface between rGO and perovskite nanosheets.

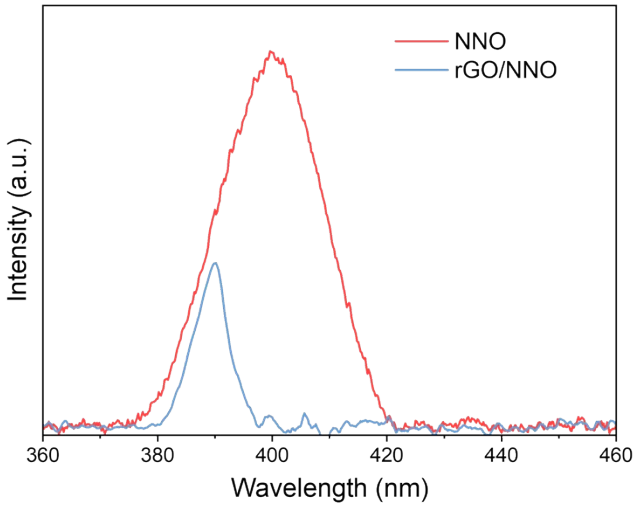

Figure S12. Steady-state fluorescence spectra with light excitation at 375nm at room temperature for NNO nanosheet which indicates the absorption maxima at 400nm while the absorption maxima at rGO/NNO shows a clear blue shift to 390nm. This is because all the states near CB are populated by the electrons transferred from rGO, triggering the Burstein-Moss shift in NNO.[17,18]

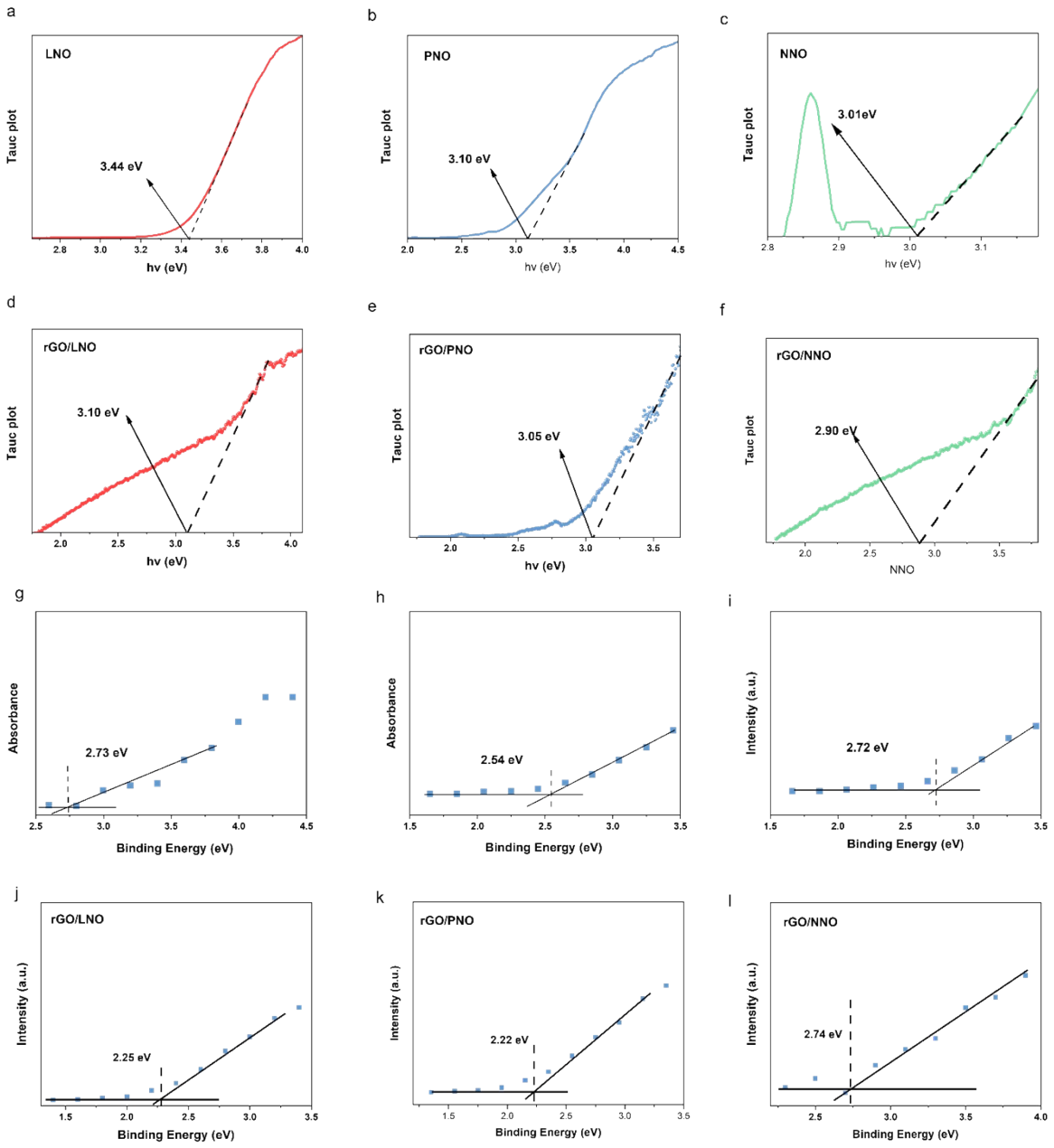

Figure.S13: Tauc plot $(F(R)*hv)^{1/2}$ of a) LNO, b) PNO, c) NNO, d) rGO/LNO, e) rGO/PNO, f) rGO/NNO; Valence band XPS of g) LNO, h) PNO, i) NNO, j) rGO/LNO, k) rGO/PNO, l) rGO/NNO

Table S1: Refined structural parameters for XRD data of $HLaNb_2O_7$ layered perovskite

Atom	Occupancy	x	y	z	$U_{iso}/Å^2$
H	1	0	0	0.5	0
La	1	0.5	0.5	0	0.001
Nb	1	0	0	0.2010	0.001
O	1	0	0.5	0.2266	0.01
O	1	0	0	0.3970	0.01
O	1	0	0	0	0.01

Table S2: Refined structural parameters for XRD data of $HPrNb_2O_7$ layered perovskite

Atom	Occupancy	x	y	z	$U_{iso}/Å^2$
H	1	0	0	0.5	0
Pr	1	0.5	0.5	0	0.001
Nb	1	0	0	0.21594	0.001
O	1	0	0.5	0.1978	0.01
O	1	0	0	0.3971	0.01
O	1	0	0	0	0.01

Table S3: Refined structural parameters for XRD data of $HNdNb_2O_7$ layered perovskite

Atom	Occupancy	x	y	z	$U_{iso}/Å^2$
H	1	0	0	0.5	0
Nd	1	0.5	0.5	0	0.001
Nb	1	0	0	0.2144	0.001
O	1	0	0.5	0.18976	0.01
O	1	0	0	0.3987	0.01
O	1	0	0	0	0.01

Table.S4: Structural parameters of the rGO/perovskite nanosheets extracted from the EXAFS fitting. CN is the coordination number; R(*Å*) is the average bond length of Nb-O; σ^2 is Debye-Waller factor. (S_0^2=0.61)

Sample	Scattering pair	CN	R(*Å*)	σ^2 ($10^{-3}Å^2$)	R factor
rGO/LNO	Nb-O	5.97 ± 0.37	2.05 ±0.006	3.0	1.46%
rGO/PNO	Nb-O	5.98 ± 0.70	2.04 ± 0.008	5.7	1.25%
rGO/NNO	Nb-O	5.77 ± 0.41	2.02 ± 0.006	2.3	2.90%

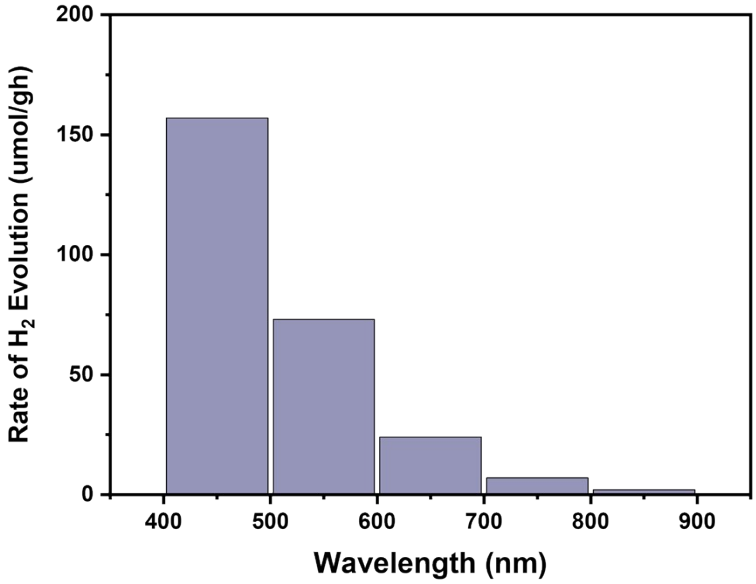

Figure.S14: HER of rGO/NNO in deionized water under different wavelengths: 400-500 (7.9 mW), 500-600 (14.1 mW), 600-700 (15.7 mW) and 700-800 nm (15.7 mW). From 400 to 800 nm, rGO/NNO shows decent activity for water splitting. In the range from 400 to 500 nm, HER activity still gives 157 μmol/gh even though the light intensity is only set at 7.9 mW.

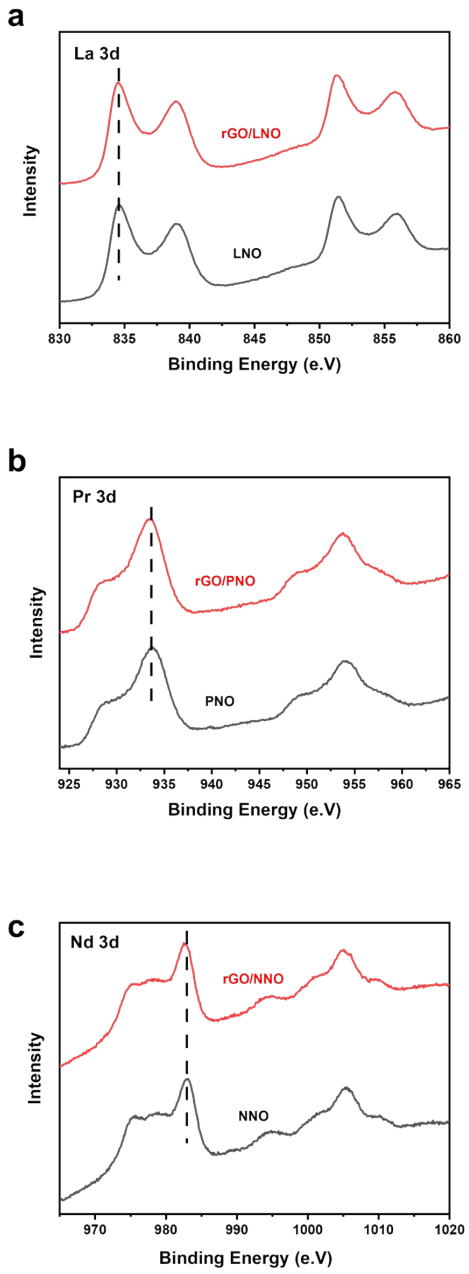

Figure.S15: a) La 3d XPS of LNO and rGO/LNO; b) Pr 3d XPS of PNO and rGO/PNO; c) Nd 3d XPS of NNO and rGO/NNO.

In LNO and rGO/LNO, the first peak of La 3d is found to be 834.5 eV. In PNO and rGO/PNO, the first peak of Pr 3d is found to be 933.7 eV. In NNO and rGO/NNO, the first peak of Nd 3d is found to be 982.9 eV. All these binding energies correspond to be the 3d of Ln^{3+} giving barely no change after incorporating with rGO.

Table S5: Performance comparison of rGO/NNO with previously reported layered perovskite photocatalysts.

Photocatalyst	HER μmol/gh	AQE	Ref
rGO/NNO	834.9 (>400 nm)	0.30% (400-500 nm)	This work
$NaLaTiO_{4-x}N_y$	~70 (>420 nm)	0.17% (400-500 nm)	19
$[Pb_8I_8(H_2O_3)][O_2C(CH_2)_4CO_2]_4$	~140 (solar simulator)	0.067% (450 nm)	20
Bi_3TiNbO_9	435.6 (>300 nm)	0.26% (365 nm)	21
$Rb_2NdNb_2O_7$	0.4 (>400 nm)	-	22
$Ca_2Ta_3O_{9.7}N_{0.2}$ nanosheet	4.7 (>420 nm)	-	8
rGO/$Ca_2Nb_3O_{10}$	820.8 (>400 nm)	-	10

$$\text{AQE} = \frac{Number\ of\ reacted\ electrons}{Number\ of\ incident\ photons} \times 100\% = \frac{2 \times Number\ of\ evolved\ H2\ molecules}{Photon\ Flux\ \times S \times t}$$

Where, S is the irradiation area, t is the photoreaction time

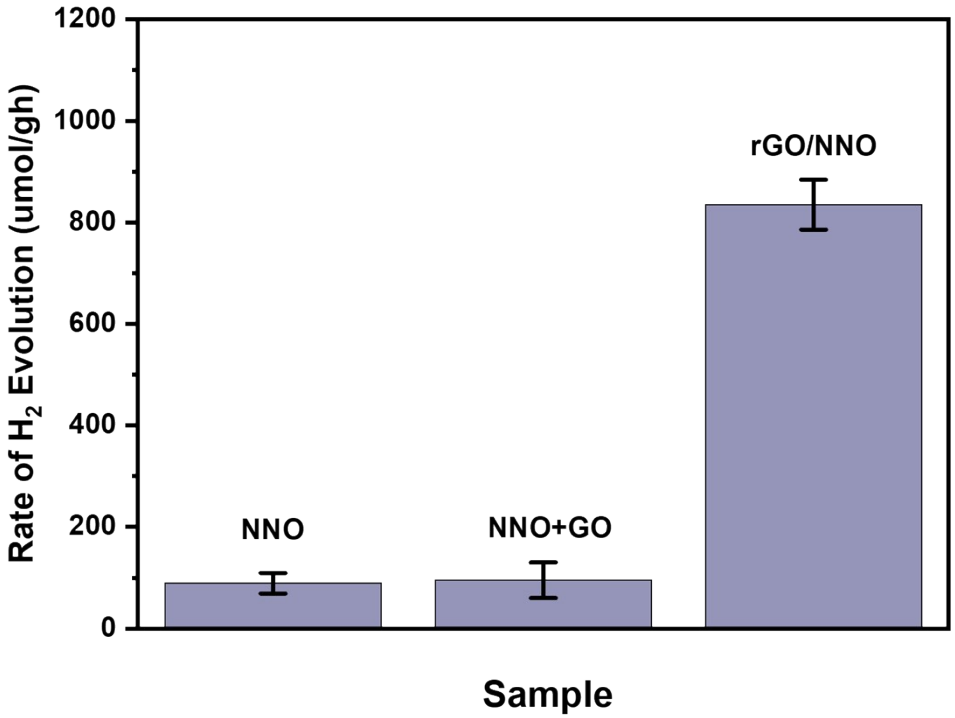

Figure.S16: The HER of NNO, physcially mixing of NNO and GO, electrostatic assembly NNO with rGO.

When NNO nanosheets are mechanically mixed with GO, the photocatalytic performance gives barely no change within experimental errors. This is because GO and NNO are not contacted with each other too well (interfacial charge transfer would not happen), and the GO would have also blocked or scattered the incident light. This result is in line with previous reports, in which perovskite nanosheets were loaded on rGO and SiO_2.[10,23]

Reference

[1] Zhu, T.; Cohen, T.; Gibbs, A. S.; Zhang, W.; Halasyamani, P. S.; Hayward, M. A.; Benedek, N. A. Theory and neutrons combine to reveal a family of layered perovskites without inversion symmetry. *Chemistry of Materials* **2017**, *29* (21), 9489-9497.

[2] Zhu, T.; Gibbs, A. S.; Benedek, N. A.; Hayward, M. A. Complex structural phase transitions of the hybrid improper polar Dion–Jacobson oxides RbNdM2O7 and CsNdM2O7 (M= Nb, Ta). *Chemistry of Materials* **2020**, *32* (10), 4340-4346.

[3] Maeda, K.; Mallouk, T. E. Comparison of two-and three-layer restacked Dion–Jacobson phase niobate nanosheets as catalysts for photochemical hydrogen evolution. *Journal of Materials Chemistry* **2009**, *19* (27), 4813-4818.

[4] Ebina, Y.; Sasaki, T.; Watanabe, M. Study on exfoliation of layered perovskite-type niobates. *Solid State Ionics* **2002**, *151* (1-4), 177-182.

[5] Kresse, G.; Furthmüller, J. Efficiency of ab-initio total energy calculations for metals and semiconductors using a plane-wave basis set. *Computational materials science* **1996**, *6* (1), 15-50.

[6] Perdew, J. P.; Burke, K.; Ernzerhof, M. Generalized gradient approximation made simple. *Physical review letters* **1996**, *77* (18), 3865.

[7] Oshima, T.; Ichibha, T.; Oqmhula, K.; Hibino, K.; Mogi, H.; Yamashita, S.; Fujii, K.; Miseki, Y.; Hongo, K.; Lu, D. Two-Dimensional Perovskite Oxynitride K2LaTa2O6N with an H+/K+ Exchangeability in Aqueous Solution Forming a Stable Photocatalyst for Visible-Light H2 Evolution. *Angewandte Chemie International Edition* **2020**, *59* (24), 9736-9743.

[8] Ida, S.; Okamoto, Y.; Matsuka, M.; Hagiwara, H.; Ishihara, T. Preparation of tantalum-based oxynitride nanosheets by exfoliation of a layered oxynitride, CsCa2Ta3O10–x N y, and their photocatalytic activity. *Journal of the American Chemical Society* **2012**, *134* (38), 15773-15782.

[9] Hojamberdiev M, Bekheet MF, Zahedi E, Wagata H, Kamei Y, Yubuta K, Gurlo A, Matsushita N, Domen K, Teshima K. New Dion–Jacobson phase three-layer perovskite CsBa2Ta3O10 and its conversion to nitrided Ba2Ta3O10 nanosheets via a nitridation–protonation–intercalation–exfoliation route for water splitting. Crystal Growth & Design. **2016**,16(4):2302-8.

[10] Li, D.; Zhao, H.; Li, L.; Mao, B.; Chen, M.; Shen, H.; Shi, W.; Jiang, D.; Lei, Y. Graphene-sensitized perovskite oxide monolayer nanosheets for efficient photocatalytic reaction. *Advanced Functional Materials* **2018**, *28* (52), 1806284.

[11] Kudo A, Kato H, Nakagawa S. Water splitting into H2 and O2 on new Sr2M2O7 (M= Nb and Ta) photocatalysts with layered perovskite structures: factors affecting the photocatalytic activity. *The Journal of Physical Chemistry B*. **2000**, 27;104(3):571-5

[12] Hasegawa T, Ueda T, Asakura Y, Yin S. Cerium (III) Niobate Layered Perovskites: Abnormal Optical Absorption Modulations by Tuning of B-Site Composition and Perovskite Layer Charge Control. Inorganic Chemistry. 2022 Dec 2;61(50):20636-46.

[13] Prasanna R, Gold-Parker A, Leijtens T, Conings B, Babayigit A, Boyen HG, Toney MF, McGehee MD. Band gap tuning via lattice contraction and octahedral tilting in perovskite materials for photovoltaics. Journal of the American Chemical Society. 2017 Aug 16;139(32):11117-24.

[14] Jiang, D.; Wang, T.; Xu, Q.; Li, D.; Meng, S.; Chen, M. Perovskite oxide ultrathin nanosheets/g-C3N4 2D-2D heterojunction photocatalysts with significantly enhanced photocatalytic activity towards the photodegradation of tetracycline. *Applied Catalysis B: Environmental.* **2017**, *201*, 617-628.

[15] Kim Y K, Park H. Light-harvesting multi-walled carbon nanotubes and CdS hybrids: Application to photocatalytic hydrogen production from water. *Energy Environ. Sci*., **2011**, 4(3): 685-694.

[16] An, J., Zhu, L., Wang, N., Song, Z., Yang, Z., Du, D., & Tang, H. Photo-Fenton like degradation of tetrabromobisphenol A with grapheneBiFeO3 composite as a catalyst. *Chemical engineering journal*, **2013**, *219*, 225-237.

[17] Shu, M.; Zhang, Z.; Dong, Z.; Xu, J. CsPbBr3 perovskite quantum dots anchored on multiwalled carbon nanotube for efficient CO2 photoreduction. *Carbon* **2021**, *182*, 454-462.

[18] Zhu Q, Lu J, Wang Y, Qin F, Shi Z, Xu C. Burstein-moss effect behind Au surface plasmon enhanced intrinsic emission of ZnO microdisks. *Scientific Reports*. **2016**, 6(1):36194.

[19] Xu, X., Wang, R., Sun, X., Lv, M. and Ni, S., 2020. Layered perovskite compound NaLaTiO4 modified by nitrogen doping as a visible light active photocatalyst for water splitting. *Acs Catalysis*, *10*(17), pp.9889-9898.

[20] Song, X., Wei, G., Sun, J., Peng, C., Yin, J., Zhang, X., Jiang, Y. and Fei, H., 2020. Overall photocatalytic water splitting by an organolead iodide crystalline material. *Nature Catalysis*, *3*(12), pp.1027-1033.

[21] Huang, J., Kang, Y., Liu, J.A., Chen, R., Xie, T., Liu, Z., Xu, X., Tian, H., Yin, L., Fan, F. and Wang, L., 2023. Selective Exposure of Robust Perovskite Layer of Aurivillius-Type Compounds for Stable Photocatalytic Overall Water Splitting. *Advanced Science*, *10*(23), p.2302206.

[22] Wakayama, H., Hibino, K., Fujii, K., Oshima, T., Yanagisawa, K., Kobayashi, Y., Kimoto, K., Yashima, M. and Maeda, K., 2019. Synthesis of a layered niobium oxynitride, Rb2NdNb2O6N· H2O, showing visible-light photocatalytic activity for H2 evolution. *Inorganic Chemistry*, *58*(9), pp.6161-6166.
[23] Zhou, H., Sabio, E.M., Townsend, T.K., Fan, T., Zhang, D. and Osterloh, F.E., 2010. Assembly of Core− Shell Structures for Photocatalytic Hydrogen Evolution from Aqueous Methanol. *Chemistry of Materials*, *22*(11), pp.3362-3368.